Local thickness-dependent permittivity model for nonlocal bounded wire-medium structures

Alexander B. Yakovlev* and Maziar Hedayati
Department of Electrical Engineering, The University of Mississippi, University, Mississippi 38677, USA

Mário G. Silveirinha
Instituto Superior Técnico, University of Lisbon and Instituto de Telecomunicações, Torre Norte, Av. Rovisco Pais 1, Lisbon 1049-001, Portugal

George W. Hanson
Department of Electrical Engineering and Computer Science, University of Wisconsin-Milwaukee, Milwaukee, Wisconsin 53211, USA
(Received 4 July 2016; published 26 October 2016)

A local thickness-dependent permittivity is derived in closed form for bounded nonlocal wire-medium structures. The model takes into account spatial dispersion (as an average per length of the wires) and the effect of the boundary, and shows that an effective local model of a nonlocal medium is thickness dependent. The permittivity is comprised of a local bulk (Drude) term and a boundary- and thickness-dependent term, the latter including the effect of spatial nonlocality. Results are obtained for different wire-medium topologies which possess strong spatial dispersion, demonstrating good agreement with a nonlocal homogenization model and full-wave simulation results.

DOI: 10.1103/PhysRevB.94.155442

I. INTRODUCTION

The interaction of electromagnetic waves with a wire medium (WM) has been of interest for a long time [1,2] and has gained attention in recent years in metamaterials research due to its ability in enabling anomalous phenomena such as negative refraction and partial focusing [3–9], subwavelength imaging of the near field [10–18], and canalization and transport of the near field to the distances of several wavelengths [19–23]. In addition, a wire medium has been utilized in various applications at microwave, terahertz, and optical frequencies [24], including high-impedance surfaces with stop-band characteristics for low-profile antennas [25–29], broadband absorbers with stable angle response [30–32], and epsilon-near-zero metamaterials [33–35], among others.

When the period of the wires is small compared to wavelength, the structure can be considered as a homogeneous (homogenized) medium. Early models of wire media neglected spatial dispersion (SD) of the homogenized material, and it has been shown that nonlocal effects are strong for wire media even in the very long wavelength limit and often cannot be ignored [36]. The usual local model takes into account only the effect of frequency dispersion in the WM and does not require additional boundary conditions (ABCs) [32,37–41] at the wire-end terminations. In Refs. [27,28,42], the role of spatial dispersion has been discussed demonstrating that nonlocal homogenization with additional boundary conditions becomes essential in the characterization of wire media. Different nonlocal homogenization methods have been developed for scattering, radiation, and excitation problems involving wire media [27,28,32,41–52].

The key property of a bounded nonlocal homogenized wire medium is that the polarization vector and the electric field are related through a spatial convolution by the susceptibility tensor $\bar{\bar{\chi}}(\mathbf{r},\mathbf{r}')$, which must incorporate information about the boundary [53]. When the material response and the field are related by a linear differential equation, a (local) Green's function for the same geometric region provides the quantity $\bar{\bar{\chi}}(\mathbf{r},\mathbf{r}')$; information about the boundary is included by enforcing the ABC on the Green's function. By elaborating on the idea presented in Ref. [53], here a local permittivity that accounts for spatial dispersion is derived in closed form for bounded WM structures. We show that the local permittivity that accounts for spatial dispersion must depend on the thickness of the wire medium (see also Ref. [54] for a discussion of metamaterial effective parameters that depend on geometry). We also note a recent model of a nonlocal metal interface where the smearing of surface charges due to nonlocal effects is approximated by a local, finite thickness layer [55]. Furthermore, the effective local permittivity developed here depends on the termination of the wires. While the approach of retrieving a thickness-dependent permittivity necessitates the solution for the nonlocal permittivity in the spatial domain, the obtained analytical expression for the local permittivity can be used directly in the local model formalism for various WM topologies, including mushroom surfaces, wire medium loaded with graphene, thin metal, or general impedance surface, bed-of-nails, and the corresponding two-sided WM structures (terminated with impedance surfaces at both interfaces). The obtained local permittivity can be useful to simplify the formulation (as a local homogenization model) for scattering, excitation, near-field, and subwavelength imaging problems. The analytical results are validated with a full-wave electromagnetic simulator, CST Microwave Studio [56], showing good agreement.

This paper is organized as follows. After a brief introduction, in Sec. II we present a general theory of boundary- and geometry-dependent local permittivity based on the Green's function approach. The closed-form expressions are obtained for the local thickness-dependent permittivity of grounded

*yakovlev@olemiss.edu

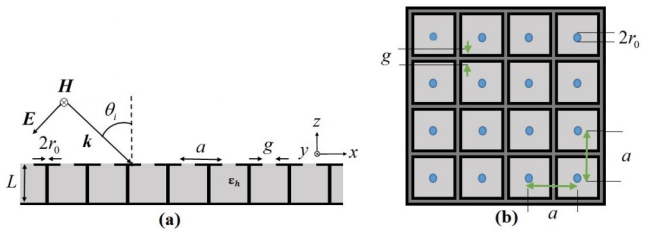

FIG. 1. Illustration of the mushroom structure with the TM-polarized plane-wave incidence. (a) Side view. (b) Top view. The structure comprises a patch array over a dielectric slab perforated with metallic vias. The periodicity of the vias and patches a, the gap between the adjacent patches g, the radius of the vias r_0, and the relative permittivity of the host medium ε_h.

and two-sided WM structures. The analytical and simulation results for plane-wave scattering from grounded and two-sided WM structures with different terminations (WM slab, WM with metallic patches, and WM loaded with graphene patches), are presented in Sec. III. The conclusions are drawn in Sec. IV. Also, the paper is accompanied by two appendices with the analytical details of nonlocal homogenization models for grounded and two-sided WM structures, included for comparison purposes. A time dependence of the form $e^{j\omega t}$ is assumed and suppressed.

II. BOUNDARY- AND GEOMETRY-DEPENDENT LOCAL PERMITTIVITY

The material response for a nontranslationally invariant, homogeneous, nonlocal medium must take into account the material boundary, and it cannot be derived simply from the bulk response. In this case, polarization and electric field are related by the susceptibility tensor $\bar{\boldsymbol{\chi}}(\mathbf{r},\mathbf{r}')$ [rather then $\bar{\boldsymbol{\chi}}(\mathbf{r}-\mathbf{r}')$ which is valid for a translationally invariant (bulk) nonlocal medium]. Alternatively, electric displacement and electric field are related by the permittivity tensor $\bar{\boldsymbol{\varepsilon}}(\mathbf{r},\mathbf{r}')$, where $\bar{\boldsymbol{\chi}}(\mathbf{r},\mathbf{r}') = \bar{\boldsymbol{\varepsilon}}(\mathbf{r},\mathbf{r}') - \mathbf{1}\delta(\mathbf{r}-\mathbf{r}')$ and $\mathbf{1}$ is the identity dyadic, such that [57,58],

$$\mathbf{D}(\mathbf{r}) = \varepsilon_0 \int \bar{\boldsymbol{\varepsilon}}(\mathbf{r},\mathbf{r}')\cdot\mathbf{E}(\mathbf{r}')d\mathbf{r}', \tag{1}$$

$$\mathbf{P}(\mathbf{r}) = \varepsilon_0 \int \bar{\boldsymbol{\chi}}(\mathbf{r},\mathbf{r}')\cdot\mathbf{E}(\mathbf{r}')d\mathbf{r}'. \tag{2}$$

In Ref. [53], the nonlocal material response that accounts for a material boundary from a macroscopic perspective is presented for a homogenized wire medium. Generalizing the spatial domain formulation for the case of a grounded WM slab terminated with an arbitrary impedance surface (with the geometry shown in Fig. 1 for a typical mushroom structure with metallic patches, or in general, patches made of 2D material as thin metal or graphene), the nonlocal homogenization satisfies the following system of equations,

$$\nabla\times\mathbf{E} = -j\omega\mu\mathbf{H}, \tag{3}$$

$$\nabla\times\mathbf{H} = \bar{\mathbf{Y}}_g\cdot\mathbf{E}\delta(z) + j\omega P_z^{\text{cond}}\hat{\mathbf{z}} + j\omega\varepsilon_0\varepsilon_h\mathbf{E}, \tag{4}$$

$$\left(k_h^2 + \frac{\partial^2}{\partial z^2}\right)P_z^{\text{cond}} = -k_p^2\varepsilon_0\varepsilon_h E_z, \tag{5}$$

where P_z^{cond} is the conduction polarization due to the z-directed wire medium,

$$P_z^{\text{cond}}(z) = \varepsilon_0\int_{-L}^{0}\chi^{\text{cond}}(z,z')E_z(z')dz'. \tag{6}$$

χ^{cond} is obviously proportional to the Green's function associated with (5), given later by (15). In (3)–(5), k_p is the plasma wave number defined as [36] $(k_p a)^2 \approx 2\pi/\ln(\frac{a^2}{4r(a-r_0)}) \approx 2\pi/(\ln(\frac{a}{2\pi r_0}) + 0.5275)$, $k_h = k_0\sqrt{\varepsilon_h}$ is the wave number of the host medium, and $\bar{\mathbf{Y}}_g$ is the surface admittance of the patch array.

By introducing a nonlocal permittivity as $\varepsilon_{\text{nonloc}}(z,z') = \chi^{\text{cond}}(z,z') + \varepsilon_h\delta(z-z')$, Ampere's law [Eq. 4] can be written in spatial integral form as

$$\nabla\times\mathbf{H} = j\omega\varepsilon_0\int_{-L}^{0}\bar{\boldsymbol{\varepsilon}}_{\text{total}}(z,z')\cdot\mathbf{E}(z')dz', \tag{7}$$

where

$$\bar{\boldsymbol{\varepsilon}}_{\text{total}}(z,z') = \frac{1}{j\omega\varepsilon_0}\bar{\mathbf{Y}}_g\delta(z)\delta(z-z') + \varepsilon_{\text{nonloc}}(z,z')\hat{\mathbf{z}}\hat{\mathbf{z}} + \varepsilon_h\delta(z-z')(\hat{\mathbf{x}}\hat{\mathbf{x}}+\hat{\mathbf{y}}\hat{\mathbf{y}}). \tag{8}$$

The nonlocal permittivity can be approximated by a local response as, $\varepsilon_{\text{nonloc}}(z,z') \approx \varepsilon_{\text{loc}}\delta(z-z')$, where ε_{loc} is the *local thickness-dependent permittivity* for a WM slab of thickness L terminated with the ground plane and the impedance surface (Fig. 1) given by

$$\varepsilon_{\text{loc}} = \frac{1}{L}\int_{-L}^{0}\int_{-L}^{0}\varepsilon_{\text{nonloc}}(z,z')dzdz'. \tag{9}$$

Then, Ampere's law can be written in a local framework as

$$\nabla\times\mathbf{H} = j\omega\varepsilon_0\bar{\boldsymbol{\varepsilon}}_{\text{total}}(z)\cdot\mathbf{E}(z), \tag{10}$$

where

$$\bar{\boldsymbol{\varepsilon}}_{\text{total}}(z) = \frac{1}{j\omega\varepsilon_0}\bar{\mathbf{Y}}_g\delta(z) + \varepsilon_{\text{loc}}\hat{\mathbf{z}}\hat{\mathbf{z}} + \varepsilon_h(\hat{\mathbf{x}}\hat{\mathbf{x}}+\hat{\mathbf{y}}\hat{\mathbf{y}}). \tag{11}$$

This is the main point of the paper. The local thickness-dependent permittivity given by (9) is understood in the averaged sense which takes into account the SD effects per length of the WM and the effect of termination. It is important to highlight that even though the thickness-dependent permittivity depends on the terminations of the metallic wires, and hence on the surroundings of the wire metamaterial, it describes *only* the response of the metallic wires, i.e., the currents induced in the metallic wires. In this regard, the surface admittance term in (11) accounts for the surface properties independent of the wire connections.

Concerning the model validity, obviously the macroscopic response of two structures (here, the wires and patches) is not generally additive when they are placed in the vicinity of one another because of near-field coupling. However, for the considered geometry we obtain accurate results since the response in the horizontal plane is determined exclusively by the currents on the patches, and the response in the vertical

direction is determined exclusively by the currents in the wires. That is, the electric response of the patches is insensitive to the presence of the wires since a horizontal electric field induces a dipole-type excitation in the patches (with currents flowing, e.g., from left to right) such that the induced current has even symmetry. This symmetry is incompatible with the excitation of currents in the vertical wires, which are associated with radial patch currents (odd-symmetry), and do not contribute to the electric dipole moment. Thus, the presence of the wires does not affect the patch surface admittance, $\bar{\mathbf{Y}}_g$. Moreover, the effective medium model of the vertical wires is intrinsically a distributed parameter model [48] with the wire array described by some equivalent inductance and capacitance per unit of length (along z). Thus, this model does not need to be corrected by the presence of the patches; the patches are treated as *loads*, similar to the usual transmission line theory. We can mention that the situation would change completely when the wires are offset with respect to the center of the patches. In this situation, a horizontal electric field can induce currents in the vertical wires, and the response of the two elements is not decoupled anymore [59]. Below we provide a summary of retrieving a local thickness-dependent permittivity for a grounded WM slab terminated with an impedance surface and then extend the approach for a general case of a two-sided WM structure.

A. The local thickness-dependent permittivity for grounded wire-medium structures

The nonlocal permittivity for a nontranslationally invariant wire medium can be given by the Green's function, $g(z,z')$, related to the material spatial dispersion and material boundary [53],

$$\varepsilon_{\text{nonloc}}(z,z') = \varepsilon_h k_p^2 g(z,z') + \varepsilon_h \delta(z-z'). \tag{12}$$

For a general case of a mushroom structure shown in Fig. 1 the Green's function is obtained as the solution of the wave equation (5) with the right-hand side replaced by $-\delta(z-z')$ subject to the ABCs at the connection of wires to the ground plane at $z=-L$ [38],

$$\left[\frac{\partial g(z,z')}{\partial z}\right]_{z=-L} = 0 \tag{13}$$

and to the impedance surface at $z=0$ [40,41,53],

$$\left[g(z,z') + \alpha\frac{\partial g(z,z')}{\partial z}\right]_{z=0} = 0, \tag{14}$$

where α depends on the patch material as detailed later, such that,

$$\begin{aligned} g(z,z') = {} & \frac{e^{-jk_h|z-z'|}}{2jk_h} - \frac{e^{jk_h(z-z')}}{2jk_h} \\ & + \frac{1}{2jk_h}\frac{1}{(1-j\alpha k_h)+(1+j\alpha k_h)e^{2jk_hL}} \\ & \times((1+j\alpha k_h)(e^{-jk_h(z+z')}+e^{jk_h(z-z'+2L)}) \\ & -(1-j\alpha k_h)(e^{-jk_h(z-z')}+e^{jk_h(z+z'+2L)})). \end{aligned} \tag{15}$$

By substituting (15) in (12) and performing the double integral (9), a closed-form expression of the local thickness-dependent permittivity can be obtained,

$$\varepsilon_{\text{loc}} = \varepsilon_h\left(1-\frac{k_p^2}{k_h^2}\right) + \varepsilon_h\frac{k_p^2}{k_h^2}\frac{\tan(k_hL)}{k_hL}\frac{1}{1-\alpha k_h\tan(k_hL)}. \tag{16}$$

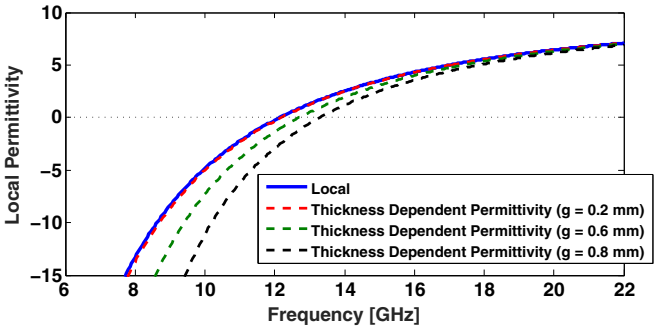

FIG. 2. Drude component (local) and thickness-dependent permittivity for a mushroom structure with different gaps. The relevant structural parameters are $a=2\,\text{mm}$, $L=1\,\text{mm}$, $r_0=0.05\,\text{mm}$, and $\varepsilon_h=10.2$.

It should be noted that (16) represents a general result for the local thickness-dependent permittivity of a grounded WM slab of thickness L terminated with an arbitrary impedance surface. Note that the impedance surface $\bar{\mathbf{Y}}_g$ is not included in ε_{loc} [see Eq. (11)], and that the local permittivity is only determined by the currents induced in the metallic wires. Due to the intrinsic nonlocality of the wire medium the currents along the wires are influenced by the surroundings via the term α, which is defined by the termination. For metallic patches, $\alpha=\frac{C_p}{C_w}$, where $C_w=\frac{2\pi\varepsilon_h\varepsilon_0}{\ln[a^2/4r_0(a-r_0)]}$ and $C_p=\frac{\pi\varepsilon_0(\varepsilon_h+1)(a-g)}{\ln[\sec(\pi g/2a)]}$ [48], and for graphene (or graphene patches), $\alpha=\frac{\sigma_s}{j\omega\varepsilon_0\varepsilon_h}$ [41]. It can be seen that the first term in (16) is the usual local permittivity of a bulk wire medium (Drude permittivity), and the second thickness-dependent term carries information about the wire connections and the averaged spatial dispersion in wire medium per length L. The presence of the second term is essential to the correct interpretation of averaged spatial dispersion and the effect of the termination in the local thickness-dependent permittivity of the wire medium.

Fig. 2 depicts the local thickness-dependent permittivity (16) for typical design parameters and different gaps of the mushroom structure, as well as the corresponding bulk Drude component ("Local") of ε_{loc} (first term in the right-hand side of Eq. (16)). As seen, an increase in the value of the gap affects the thickness-dependent permittivity, such that the effective plasma frequency is increased. In the limit of a very small gap, $\alpha\to\infty$ (which corresponds to replacing the impedance surface by a perfect electric conductor (PEC)), the thickness-dependent permittivity (16) reduces to the Drude component, such that for the electrically short wires in the presence of PEC ground planes at $z=-L$ and $z=0$ the second term in (16) vanishes.

To highlight how the termination can dramatically affect ε_{loc}, we consider the special case of $\alpha\to 0$, which corresponds

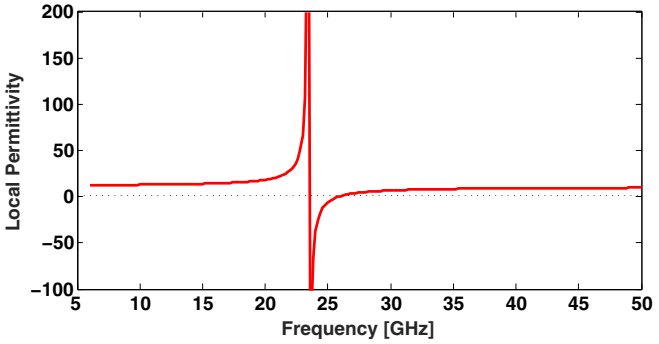

FIG. 3. Local thickness-dependent permittivity for a bed-of-nails with short wires. The relevant structural parameters are $a = 2$ mm, $L = 1$ mm, $r_0 = 0.05$ mm, and $\varepsilon_h = 10.2$.

to the bed-of-nails structure (with the impedance surface removed in Fig. 1). Then, the local thickness-dependent permittivity (16) reduces to

$$\varepsilon_{\rm loc} = \varepsilon_h\left(1 - \frac{k_p^2}{k_h^2}\right) + \varepsilon_h \frac{k_p^2}{k_h^2}\frac{\tan(k_h L)}{k_h L}. \tag{17}$$

A typical variation of $\varepsilon_{\rm loc}$ as a function of frequency is depicted in Fig. 3. Interestingly, when the patch terminations are removed the pole in the permittivity dispersion at zero frequency disappears. In the static limit, $k_h L \to 0$, the local thickness-dependent permittivity for the bed-of-nails (17) is bounded by the host permittivity ε_h. Also, for electrically short wires, $k_h L \leqslant 1$, it can be seen that $\varepsilon_{\rm loc}$ is positive independent of the value of k_p, and that it asymptotically approaches infinity at the Fabry-Pérot resonance condition, $k_h L = \pi/2$.

With the obtained analytical expression of the local thickness-dependent permittivity (16) the solution of the TM-polarized plane-wave scattering from the mushroom structure (Fig. 1) naturally falls into the simple local model framework where the reflection coefficient is obtained for an equivalent homogeneous grounded slab (uniaxial anisotropic crystal characterized by the local thickness-dependent permittivity (16) in the z direction) loaded with the patch array as follows [27],

$$R = \frac{\frac{\varepsilon_h}{\gamma_{\rm loc}}\coth(\gamma_{\rm loc} L) + \frac{\eta_0}{jk_0}Y_g - \frac{1}{jk_z}}{\frac{\varepsilon_h}{\gamma_{\rm loc}}\coth(\gamma_{\rm loc} L) + \frac{\eta_0}{jk_0}Y_g + \frac{1}{jk_z}}, \tag{18}$$

where

$$\gamma_{\rm loc} = \sqrt{\frac{\varepsilon_h k_x^2}{\varepsilon_{\rm loc}} - k_h^2}, \tag{19}$$

with $\eta_0 = \sqrt{\mu_0/\varepsilon_0}$ being the intrinsic impedance of free space, $k_z = k_0\cos(\theta_i)$, and Y_g is determined by (24) for metallic patches and (25) for graphene patches. For a bed-of-nails, $\varepsilon_{\rm loc}$ is given by (17) and $Y_g = 0$ in (18).

B. The local thickness-dependent permittivity for two-sided wire-medium structures

Here, we extend the analysis to a general case of a WM two-sided structure loaded with metallic or graphene patches (with the geometry shown in Fig. 4), or in general with an arbitrary

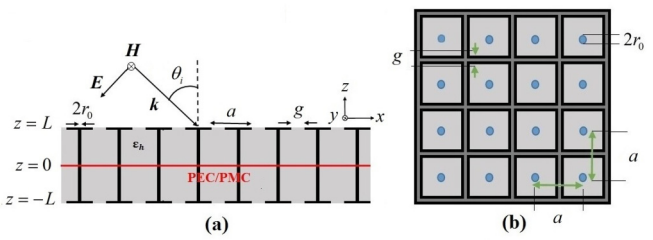

FIG. 4. Schematics of a WM two-sided structure loaded with metallic or graphene patches: (a) cross-section view of the structure by considering a perfect electric conductor (PEC)/perfect magnetic conductor (PMC) symmetry plane, (b) top view.

impedance surface, illuminated by a TM-polarized uniform plane wave obliquely incident at an angle θ_i. The metallic wires are oriented along the z direction and patches are located at $z = -L$ and $z = L$. Due to the symmetry (PEC/PMC ground plane at $z = 0$) Green's function problems are formulated with the even and odd excitation, respectively. For the even excitation the Green's function g_e is the solution of the wave equation (5) with the source $\delta(z - z') + \delta(z + z')$, and for the odd excitation the Green's function g_o is due to $\delta(z - z') - \delta(z + z')$. By applying the superposition principle we can obtain the Green's function for the entire WM slab as $g = (g_e + g_o)/2$. The local thickness-dependent permittivity can be expressed in terms of even and odd local permittivities/susceptibilities,

$$\begin{aligned}\varepsilon_{\rm nonloc}(z,z') &= \frac{\varepsilon_{\rm nonloc(e)}(z,z') + \varepsilon_{\rm nonloc(o)}(z,z')}{2} \\ &= \frac{\chi_e(z,z') + \chi_o(z,z')}{2} + \varepsilon_h\delta(z - z'),\end{aligned} \tag{20}$$

where $\chi_e(z,z') = \varepsilon_h k_p^2 g_e(z,z')$ and $\chi_o(z,z') = \varepsilon_h k_p^2 g_o(z,z')$. Note that g_e coincides with the Green function introduced in the previous section when both z and z' are positive.

By relating the nonlocal and local permittivities as $\varepsilon_{\rm nonloc}(z,z') = \varepsilon_{\rm loc}\delta(z - z')$, the local thickness-dependent permittivity of the entire WM slab is obtained,

$$\varepsilon_{\rm loc} = \frac{1}{2L}\int_{-L}^{L}\int_{-L}^{L}\varepsilon_{\rm nonloc}(z,z')dzdz', \tag{21}$$

where $\varepsilon_{\rm nonloc}(z,z')$ is given by (20). It is noted that $\chi_o(z,z')$ is an odd function of both z and z' and does not contribute to the double integral in (21). Consequently, (21) leads to the same closed-form expression (16) that was obtained for the grounded WM structure, such that the local thickness-dependent permittivity of the entire WM slab of thickness $2L$ is the same as the one for a grounded WM slab of thickness L.

The two-sided WM structure in Fig. 4 can thus be replaced by an equivalent local uniaxial dielectric slab with thickness-dependent permittivity (16) in the z direction and loaded with patches on both sides at $z = -L$ and $z = L$ as shown in Fig. 5. The solution of the scattering problem with the TM-polarized plane-wave incidence is obtained in the local model framework. The total magnetic fields in the air regions

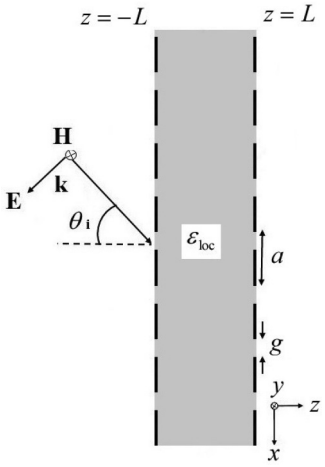

FIG. 5. Local homogenization model of the WM slab loaded with metallic or graphene patches.

and the WM slab (Fig. 5) can be expressed as follows,

$$Hy = \begin{cases} e^{-jk_z(z+L)} + Re^{jk_z(z+L)} & z < -L \\ A^+e^{-\gamma_{\rm loc}z} + A^-e^{\gamma_{\rm loc}z} & -L \leqslant z \leqslant L \\ Te^{-jk_z(z-L)} & z > L \end{cases}, \tag{22}$$

where R and T are the reflection and transmission coefficients and $\gamma_{\rm loc}$ is defined by (19). The corresponding electric field is obtained from the Maxwell's equations.

By applying the sheet impedance boundary conditions at $z = -L$ and $z = L$ (as continuous tangential electric field and discontinuous tangential magnetic field in the value of surface reactance given by (24) for metallic patches and (25) for graphene patches), the following system of linear equations is obtained,

$$\begin{pmatrix} jk_z\varepsilon_h & \gamma_{\rm loc}e^{\gamma_{\rm loc}L} & -\gamma_{\rm loc}e^{-\gamma_{\rm loc}L} & 0 \\ 0 & \gamma_{\rm loc}e^{-\gamma_{\rm loc}L} & -\gamma_{\rm loc}e^{\gamma_{\rm loc}L} & -jk_z\varepsilon_h \\ 1+\frac{k_zY_g}{\omega\varepsilon_0} & -e^{\gamma_{\rm loc}L} & -e^{-\gamma_{\rm loc}L} & 0 \\ 0 & e^{-\gamma_{\rm loc}L} & e^{\gamma_{\rm loc}L} & -\left(1+\frac{k_zY_g}{\omega\varepsilon_0}\right) \end{pmatrix} \times \begin{pmatrix} R \\ A^+ \\ A^- \\ T \end{pmatrix} = \begin{pmatrix} jk_z\varepsilon_h \\ 0 \\ \frac{k_zY_g}{\omega\varepsilon_0}-1 \\ 0 \end{pmatrix}, \tag{23}$$

which can be solved either numerically or analytically for the unknown field coefficients R, T, and $A^{\pm}$.

III. RESULTS AND DISCUSSIONS

In the following, we present a comparative study of the reflection/transmission for grounded (Fig. 1) and two-sided WM (Fig. 4) structures obtained with local and nonlocal homogenization models. Also, all the homogenization model results are verified with the full-wave commercial software, CST Microwave Studio [56], showing good agreement. In the following, $\bar{\mathbf{Y}}_g = (\hat{\mathbf{x}}\hat{\mathbf{x}} + \hat{\mathbf{y}}\hat{\mathbf{y}})Y_g$ is the surface admittance of the patch array for transverse magnetic (TM) waves, obtained in closed form for metallic elements [60],

$$Y_g = j\varepsilon_0(\varepsilon_h + 1)(\omega a/\pi)\ln[\csc(\pi g/2a)] \tag{24}$$

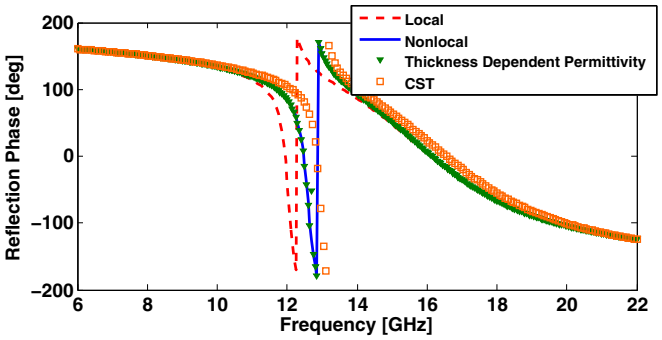

FIG. 6. Reflection phase calculated with the nonlocal, local (Drude)), and local thickness-dependent permittivity models for a mushroom surface with $a = 2\,\text{mm}$, $L = 1\,\text{mm}$, $r_0 = 0.05\,\text{mm}$, $g = 0.6\,\text{mm}$, $\theta_i = 30^o$, and $\varepsilon_h = 10.2$.

and for graphene patches [41],

$$Y_g = \left(\frac{a}{(a-g)\sigma_s} - \frac{j\pi}{\omega\varepsilon_0(\varepsilon_h+1)a\ln(\csc(\pi g/2a))}\right)^{-1}, \tag{25}$$

where σ_s is the complex surface conductivity of graphene obtained with the Kubo formula [61]. Closed-form expressions for the intraband and interband contributions in the surface conductivity are given in Appendix A.

In order to demonstrate the performance of the proposed local thickness-dependent permittivity we begin with the analysis of the reflection phase of the grounded mushroom structure with metallic patches shown in Fig. 1. An example of a mushroom structure with electrically short wires, $k_hL \leqslant 1$, and $L/a \leqslant 1$, is considered with the TM-polarized plane-wave incidence at 30 degrees, with $a = 2\,\text{mm}$, $L = 1\,\text{mm}$, $r_0 = 0.05\,\text{mm}$, $g = 0.6\,\text{mm}$, and $\varepsilon_h = 10.2$. The corresponding frequency dispersion of $\varepsilon_{\rm loc}$ is represented in Fig. 2.

In Fig. 6, the reflection phase behavior is shown based on the solution of local and nonlocal homogenization models, where the results of local thickness-dependent permittivity model are obtained with (18) and nonlocal model results are generated with (A3)–(A5) provided in Appendix A. The results of the local model are obtained also with (18) with the local Drude permittivity function (see Fig. 2). It can be seen that the results of local thickness-dependent permittivity and nonlocal

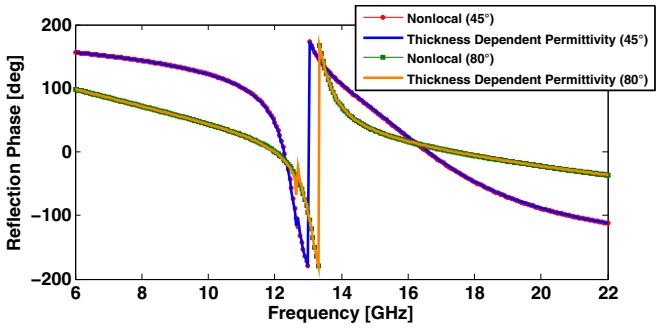

FIG. 7. Reflection phase calculated with the nonlocal and local thickness-dependent permittivity models for a mushroom surface at different angles of incidence with $a = 2\,\text{mm}$, $L = 1\,\text{mm}$, $r_0 = 0.05\,\text{mm}$, $g = 0.6\,\text{mm}$, and $\varepsilon_h = 10.2$.

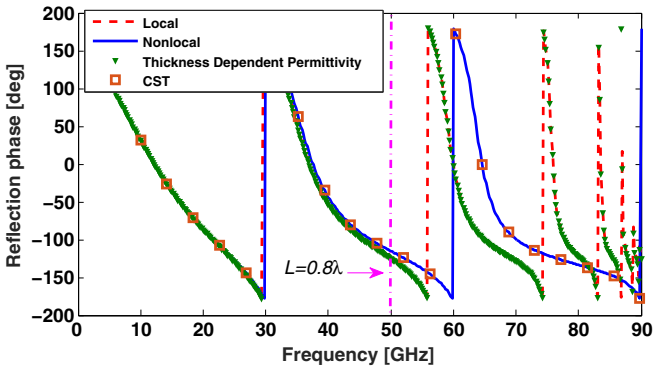

FIG. 8. Reflection phase calculated with the nonlocal, local (Drude), and local thickness-dependent permittivity models for a mushroom structure with $a = 1$ mm, $g = 0.1$ mm, $L = 5$ mm, $r_0 = 0.05$ mm, $\theta_i = 30^o$, and $\varepsilon_h = 1$.

homogenization models are in perfect agreement for the entire frequency range. The two local models (the simple Drude model and the thickness-dependent permittivity model) yield a resonant behavior when the permittivity crosses zero. Clearly, the simple Drude model is inaccurate and erroneously predicts

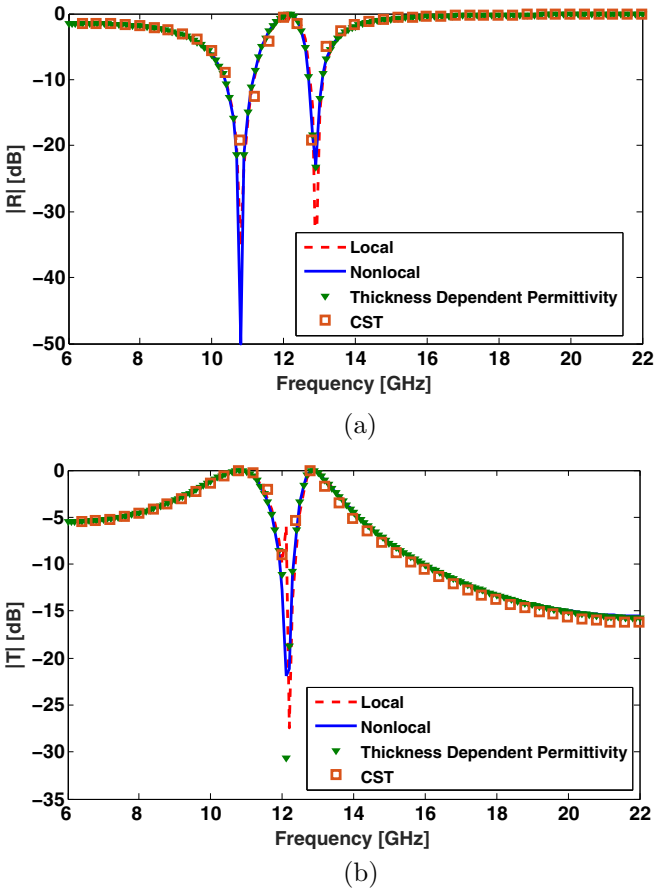

FIG. 9. Magnitude of the (a) reflection and (b) transmission coefficients calculated with nonlocal, local (Drude), and local thickness dependent permittivity models for a two-sided mushroom structure with metallic patches for the following parameters: $a = 2$ mm, $2L = 2$ mm, $r_0 = 0.05$ mm, $\theta_i = 30^o$, $g = 0.2$ mm, and $\varepsilon_h = 10.2$.

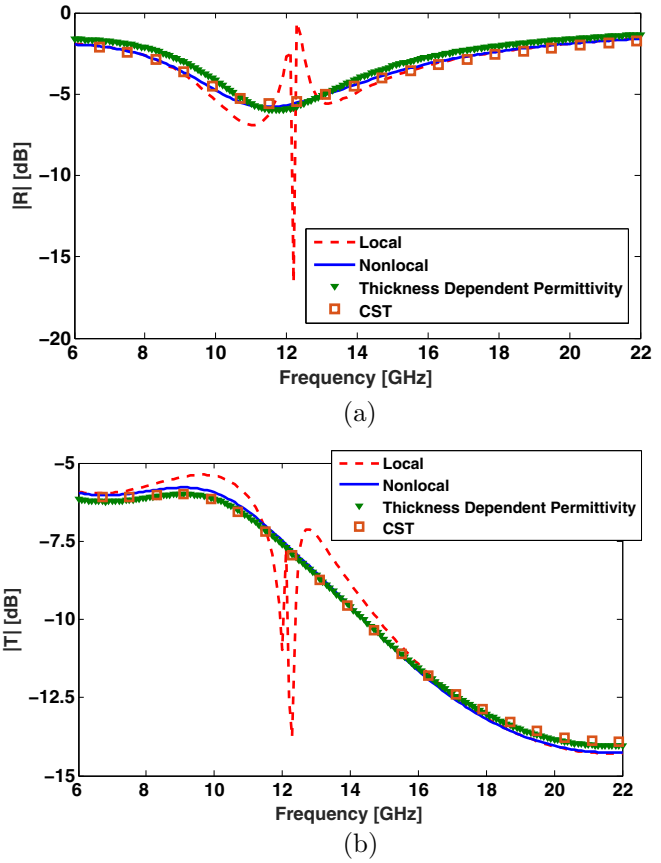

FIG. 10. Magnitude of the (a) reflection and (b) transmission coefficients calculated with nonlocal, local (Drude), and local thickness dependent permittivity models for a two-sided mushroom structure loaded with graphene patches for the following parameters: $a = 2$ mm, $g = 0.2$ mm, $2L = 2$ mm, $r_0 = 0.05$ mm, $\varepsilon_h = 10.2$, $\theta_i = 30^o$, $T = 300$ K, $\tau = 0.35$ ps, and $\mu_c = 0.5$ eV.

that the plasma resonance occurs at 12.14 GHz. In this example a moderate value of the gap between the patches, 0.6 mm, is used in order to demonstrate that spatial dispersion effects are not negligible and our model of local thickness-dependent permittivity accurately captures the correct physical behavior of the structure. Also, in Fig. 7 it is shown for the example of a mushroom surface with short wires that the local thickness-dependent permittivity model gives accurate results for larger angles of incidence in the entire frequency.

As another example, we consider a mushroom structure with $a = 1$ mm, $g = 0.1$ mm, $L = 5$ mm, $r_0 = 0.05$ mm, and $\varepsilon_h = 1$, such that $L/a \gg 1$. In Fig. 8, the reflection phase is obtained with the local thickness-dependent permittivity model and compared with the results of nonlocal and local (Drude) models. It can be seen that for the case of long wires, $L/a \gg 1$, both local models predict the correct physical behavior at lower frequencies and up to 50 GHz, even when the length of the wires is a significant fraction of wavelength, $L = 0.8\lambda_0$, due to extreme anisotropy of wire medium with long wires [42].

Next, the reflection/transmission response is studied for several representative two-sided WM topologies shown in Fig. 4. The results of the local thickness-dependent permittivity

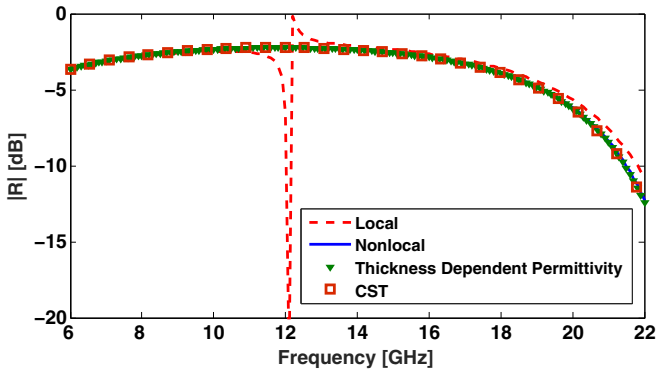

(a)

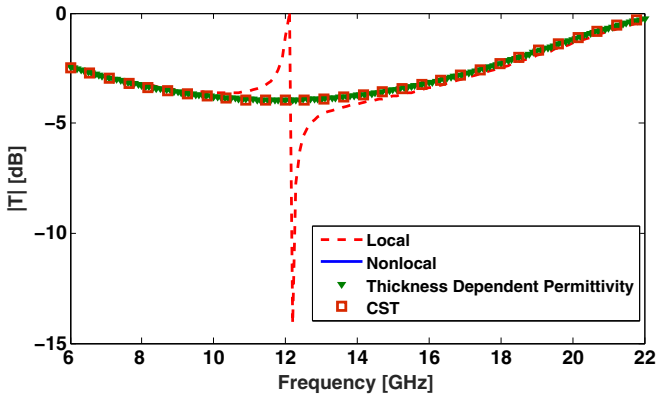

(b)

FIG. 11. Magnitude of the (a) reflection and (b) transmission coefficients calculated with nonlocal, local (Drude), and local thickness dependent permittivity models for a WM slab for the following parameters: $a = 2\,\text{mm}$, $2L = 2\,\text{mm}$, $r_0 = 0.05\,\text{mm}$, $\varepsilon_h = 10.2$, and $\theta_i = 30^\circ$.

model [as the solution of (23)] are compared with nonlocal homogenization model results (with the formulation given in Appendix B), showing good agreement. Also, for comparison the results of the local (Drude) permittivity model are included.

In Fig. 9, the reflection and transmission coefficients are plotted for a two-sided mushroom structure with metallic patches for a TM-polarized plane wave incident at 30 degrees. It can be seen that the results of the model with the local thickness-dependent permittivity are in perfect agreement with the nonlocal homogenization model results for the entire frequency range. The local (Drude) model also accurately predicts the reflection/transmission behavior because in this example a small value of the gap ($g = 0.2\,\text{mm}$) is used, such that spatial dispersion is significantly reduced in the wire medium in the presence of metallic patches [27].

The reflection/transmission response of a two-sided mushroom structure loaded with graphene patches is shown in Fig. 10, demonstrating good agreement between the results of local thickness-dependent permittivity and nonlocal homogenization models. Graphene's complex surface conductivity is modeled with the Kubo formula [61] and both intraband and interband contributions are used in the calculations with $T = 300\,\text{K}$, $\tau = 0.35\,\text{ps}$, and $\mu_c = 0.5\,\text{eV}$. This example clearly demonstrates that the local (Drude) model results fail to accurately predict the reflection and transmission behavior (especially, close to the plasma frequency of 12.14 GHz) due to strong spatial dispersion in wire medium in the presence of graphene patches (due to finite surface conductivity of graphene).

The example of a WM slab (geometry in Fig. 4 with the impedance surfaces removed) is studied for a TM-polarized plane wave incident at 30 degrees. Again, excellent agreement is obtained in Fig. 11 between the results of local thickness-dependent permittivity and nonlocal homogenization models, whereas the local (Drude) model fails close to the plasma frequency due to strong spatial dispersion in the wire medium.

As a summary, the local thickness-dependent permittivity model for grounded and two-sided WM structures with an arbitrary surface impedance gives accurate results for reflection/transmission for WM structures with short wires, $L/a \leqslant 1$, at low frequencies (electrically short wires, $k_h L \leqslant 1$), and for WM structures with long wires, $L/a \gg 1$, at low and higher frequencies when the length of the wires is comparable to the wavelength in free space (due to extreme anisotropy of the wire medium with long wires).

IV. CONCLUSION

A local thickness-dependent permittivity has been derived in closed form for bounded nonlocal WM structures, taking into account spatial dispersion (as an average per length of wires) and the effects of the wire terminations. The results of the local thickness-dependent permittivity model are in good agreement with the results of nonlocal homogenization model for grounded and two-sided WM structures with arbitrary terminations. The obtained closed-form expressions for local thickness-dependent permittivity simplify the formulation and can be used in the local model formalism for scattering, excitation, near-field, and subwavelength imaging problems involving wire medium. This simplified effective medium description can be useful to model complex wire media structures as a continuum in commercial electromagnetic solvers. Furthermore, our theory highlights that thickness-dependent effective parameters - a common feature of electromagnetic metamaterials - may result from spatially dispersive effects.

ACKNOWLEDGMENT

The authors are thankful to Gabriel Moreno and Ali Forouzmand for their help with numerical simulations.

APPENDIX A: NONLOCAL HOMOGENIZATION MODEL FOR GROUNDED WIRE-MEDIUM STRUCTURES

To provide a comparison to the thickness-dependent effective local permittivity, here we consider a grounded WM structure shown in Fig. 1. In the nonlocal homogenization model, a wire medium is characterized by a uniaxial anisotropic material with the nonlocal effective permittivity along the wires as $\varepsilon_{\text{nonloc}} = [1 - k_p^2/(k_h^2 - k_z^2)]$, where $k_h = k_0\sqrt{\varepsilon_h}$ is the wavenumber of the host medium, $k_0 = \omega/c$ is the free space wavenumber, ω is the angular frequency, c is the speed of light, k_z is the z-component of the wave vector $\mathbf{k} = (k_x, 0, k_z)$, and k_p is the plasma wave number. A TM-polarized plane wave excites both extraordinary transverse electromagnetic (TEM)

and the transverse magnetic (TM) modes in the homogenized WM slab. The total magnetic fields in the air region above the structure (region 1) and in the WM slab (region 2) can be written as follows,

$$H_y^{(1)} = (e^{\gamma_0 z} + Re^{-\gamma_0 z})e^{-jk_x x}, \tag{A1}$$

$$H_y^{(2)} = (A_{\rm TM}^{+}e^{\gamma_{\rm TM} z} + A_{\rm TM}^{-}e^{-\gamma_{\rm TM} z} + B_{\rm TEM}^{+}e^{\gamma_{\rm TEM} z} + B_{\rm TEM}^{-}e^{-\gamma_{\rm TEM} z})e^{-jk_x x}, \tag{A2}$$

where $A_{\rm TM}^{\pm}$ and $B_{\rm TEM}^{\pm}$ are the amplitudes of TM and TEM modes in the WM slab, R is the reflection coefficient, $\gamma_0=\sqrt{k_x^2-k_0^2}$, $k_x = k_0\sin\theta_i$ is the x-component of the wave vector $\mathbf{k}$, and $\gamma_{\rm TM}=\sqrt{k_p^2+k_x^2-k_h^2}$. In order to determine the unknown amplitude coefficients the ABCs [38,40,41] are enforced at the connection of wires to the ground plane and to the metallic patches along with the sheet impedance boundary conditions across the patch array interface, resulting in the analytical expression for the reflection coefficient,

$$R = \frac{\frac{N}{D}\coth(\gamma_{\rm TM}L)\cot(k_hL) - \left(\frac{1}{\gamma_0} + j\frac{\eta_0 Y_g}{k_0}\right)}{\frac{N}{D}\coth(\gamma_{\rm TM}L)\cot(k_hL) + \left(\frac{1}{\gamma_0} - j\frac{\eta_0 Y_g}{k_0}\right)}, \tag{A3}$$

$$N = \left(\frac{1}{\varepsilon_{zz}^{\rm TM}} - 1\right)\left(\frac{C_p\gamma_{\rm TM}}{C_w}\tanh(\gamma_{\rm TM}L) + 1\right) + \left(1 - \frac{C_pk_h}{C_w}\tan(k_hL)\right), \tag{A4}$$

$$D = -\frac{k_h}{\varepsilon_h}\left(\frac{1}{\varepsilon_{zz}^{\rm TM}} - 1\right)\left(\frac{C_p\gamma_{\rm TM}}{C_w} + \coth(\gamma_{\rm TM}L)\right) + \frac{\gamma_{\rm TM}}{\varepsilon_h}\left(\cot(k_hL) - \frac{C_pk_h}{C_w}\right), \tag{A5}$$

where $\varepsilon_{zz}^{\rm TM} = [1 - k_p^2/(k_x^2 + k_p^2)]$.

In the case of WM terminated with graphene patches formulation is the same with $\frac{C_p}{C_w}$ replaced by $\frac{\sigma_s}{j\omega\varepsilon_0\varepsilon_h}$ in (A3)–(A5) [17,41]. Graphene's complex surface conductivity σ_s is modeled with the Kubo formula using closed-form expressions for the interband $\sigma_{\rm inter}$ and intraband $\sigma_{\rm intra}$ contributions [61],

$$\sigma_{\rm intra} = -j\frac{k_Be^2T}{\pi\hbar^2(\omega - j\tau^{-1})}\left(\frac{\mu_c}{Tk_B} + 2\ln(e^{-\frac{\mu_c}{Tk_B}}+1)\right), \tag{A6}$$

$$\sigma_{\rm inter} \approx -\frac{je^2}{4\pi\hbar}\ln\left(\frac{2|\mu_c| - \omega\hbar}{2|\mu_c| + \omega\hbar}\right), \tag{A7}$$

$$\sigma_s = \sigma_{\rm intra} + \sigma_{\rm inter}. \tag{A8}$$

APPENDIX B: NONLOCAL HOMOGENIZATION MODEL FOR TWO-SIDED WIRE-MEDIUM STRUCTURES

In order to determine the transmission/reflection response of the two-sided WM structure with a TM plane-wave excitation, the even/odd excitation technique is utilized (due to symmetry of the structure with PEC/PMC planes as shown in Fig. 4). The nonlocal homogenization model for the even excitation (PEC symmetry) is the same as for a grounded WM structure considered in Appendix A (closed-form expressions (A3)–(A5) for the reflection coefficient). For the odd excitation (PMC symmetry) the formulation is similar with the ABC at the PMC ground plane corresponding to the open-end wire termination [42]. The closed-form expressions of the reflection coefficient with the odd excitation are obtained as follows,

$$R_o = \frac{\frac{N_o}{D_o}\tanh(\gamma_{\rm TM}L)\tan(k_hL) - \left(\frac{1}{\gamma_0} + j\frac{\eta_0}{Z_gk_0}\right)}{\frac{N_o}{D_o}\tanh(\gamma_{\rm TM}L)\tan(k_hL) + \left(\frac{1}{\gamma_0} - j\frac{\eta_0}{Z_gk_0}\right)}, \tag{B1}$$

$$N_o = \left(\frac{1}{\varepsilon_{zz}^{\rm TM}} - 1\right)\left(\frac{C_p\gamma_{\rm TM}}{C_w}\coth(\gamma_{\rm TM}L) + 1\right) + \left(1 + \frac{C_pk_h}{C_w}\cot(k_hL)\right), \tag{B2}$$

$$D_o = \frac{k_h}{\varepsilon_h}\left(\frac{1}{\varepsilon_{zz}^{\rm TM}} - 1\right)\left(\frac{C_p\gamma_{\rm TM}}{C_w} + \tanh(\gamma_{\rm TM}L)\right) + \frac{\gamma_{\rm TM}}{\varepsilon_h}\left(\tan(k_hL) + \frac{C_pk_h}{C_w}\right). \tag{B3}$$

The transmission/reflection response of the structure can be obtained by the superposition principle as $R = \frac{1}{2}(R_e + R_o)$ and $T = \frac{1}{2}(R_e - R_o)$. In the case of graphene patches $\frac{C_p}{C_w}$ is replaced by $\frac{\sigma_s}{j\omega\varepsilon_0\varepsilon_h}$.

[1] J. Brown, Prog. Dielectr. **2**, 195 (1960).
[2] W. Rotman, IRE Trans. Antennas Propagat. **10**, 82 (1962).
[3] M. G. Silveirinha, Phys. Rev. B **79**, 153109 (2009).
[4] M. G. Silveirinha and A. B. Yakovlev, Phys. Rev. B **81**, 233105 (2010).
[5] C. S. R. Kaipa, A. B. Yakovlev, and M. G. Silveirinha, J. Appl. Phys. **109**, 044901 (2011).
[6] C. S. R. Kaipa, A. B. Yakovlev, S. I. Maslovski, and M. G. Silveirinha, Phys. Rev. B **84**, 165135 (2011).
[7] T. A. Morgado, S. I. Maslovski, and M. G. Silveirinha, New J. Phys. **14**, 063002 (2012).
[8] T. A. Morgado, J. S. Marcos, S. I. Maslovski, and M. G. Silveirinha, Appl. Phys. Lett. **101**, 021104 (2012).
[9] C. S. R. Kaipa and A. B. Yakovlev, J. Appl. Phys. **112**, 124902 (2012).
[10] P. A. Belov and M. G. Silveirinha, Phys. Rev. E **73**, 056607 (2006).
[11] P. A. Belov, Y. Hao, and S. Sudhakaran, Phys. Rev. B **73**, 033108 (2006).
[12] M. G. Silveirinha, P. A. Belov, and C. R. Simovski, Phys. Rev. B **75**, 035108 (2007).
[13] M. G. Silveirinha, P. A. Belov, and C. R. Simovski, Opt. Lett. **33**, 1726 (2008).
[14] M. G. Silveirinha, C. R. Medeiros, C. A. Fernandes, and J. R. Costa, Phys. Rev. B **81**, 033101 (2010).
[15] T. A. Morgado, J. S. Marcos, M. G. Silveirinha, and S. I. Maslovski, Appl. Phys. Lett. **97**, 144102 (2010).
[16] C. S. R. Kaipa, A. B. Yakovlev, S. I. Maslovski, and M. G. Silveirinha, Phys. Rev. B **86**, 155103 (2012).
[17] A. Forouzmand and A. B. Yakovlev, AIP Adv. **5**, 077108 (2015).

[18] A. Forouzmand, H. M. Bernety, and A. B. Yakovlev, Phys. Rev. B **92**, 085402 (2015).

[19] P. A. Belov, C. R. Simovski, and P. Ikonen, Phys. Rev. B **71**, 193105 (2005).

[20] P. A. Belov, Y. Zhao, S. Tse, P. Ikonen, M. G. Silveirinha, C. R. Simovski, S. A. Tretyakov, Y. Hao, and C. G. Parini, Phys. Rev. B **77**, 193108 (2008).

[21] P. Ikonen, C. R. Simovski, S. A. Tretyakov, P. A. Belov, and Y. Hao, Appl. Phys. Lett. **91**, 104102 (2007).

[22] T. A. Morgado and M. G. Silveirinha, New J. Phys. **11**, 083023 (2009).

[23] Y. Zhao, G. Palikaras, P. A. Belov, R. F. Dubrovka, C. R. Simovski, Y. Hao, and C. G. Parini, New J. Phys. **12**, 103045 (2010).

[24] C. R. Simovski, P. A. Belov, A. V. Atrashchenko, and Yu. S. Kivshar, Adv. Mater. **24**, 4229 (2012).

[25] D. F. Sievenpiper, L. Zhang, R. Broas, N. Alexopolous, and E. Yablonovitch, IEEE Trans. Microwave Theory Tech. **47**, 2059 (1999).

[26] F. Yang and Y. Rahmat-Samii, IEEE Trans. Antennas Propagat. **51**, 2691 (2003).

[27] O. Luukkonen, M. G. Silveirinha, A. B. Yakovlev, C. R. Simovski, I. S. Nefedov, and S. A. Tretyakov, IEEE Trans. Microw. Theory Tech. **57**, 2692 (2009).

[28] A. B. Yakovlev, M. G. Silveirinha, O. Luukkonen, C. R. Simovski, I. S. Nefedov, and S. A. Tretyakov, IEEE Trans. Microw. Theory Tech. **57**, 2700 (2009).

[29] C. S. R. Kaipa, A. B. Yakovlev, S. I. Maslovski, and M. G. Silveirinha, IEEE Antennas Wireless Propagat. Lett. **10**, 1503 (2011).

[30] S. A. Tretyakov and S. I. Maslovski, Microw. Opt. Technol. Lett. **38**, 153 (2003).

[31] O. Luukkonen, F. Costa, C. R. Simovski, A. Monorchio, and S. A. Tretyakov, IEEE Trans. Antennas Propagat. **57**, 3119 (2009).

[32] Y. R. Padooru, A. B. Yakovlev, C. S. R. Kaipa, G. W. Hanson, F. Medina, F. Mesa, and A. W. Glisson, IEEE Trans. Antennas Propagat. **60**, 5727 (2012).

[33] M. Silveirinha and N. Engheta, Phys. Rev. Lett. **97**, 157403 (2006).

[34] E. Forati and G. W. Hanson, New J. Phys. **15**, 123027 (2013).

[35] E. Forati, G. W. Hanson, and D. F. Sievenpiper, IEEE Trans. Antennas Propagat. **63**, 1909 (2015).

[36] P. A. Belov, R. Marques, S. I. Maslovski, I. S. Nefedov, M. G. Silveirinha, C. R. Simovski, and S. A. Tretyakov, Phys. Rev. B **67**, 113103 (2003).

[37] M. G. Silveirinha, IEEE Trans. Antennas Propagat. **54**, 1766 (2006).

[38] M. G. Silveirinha, C. A. Fernandes, and J. R. Costa, New J. Phys. **10**, 053011 (2008).

[39] M. G. Silveirinha, New J. Phys. **11**, 113016 (2009).

[40] S. I. Maslovski, T. A. Morgado, M. G. Silveirinha, C. S. R. Kaipa, and A. B. Yakovlev, New J. Phys. **12**, 113047 (2010).

[41] A. B. Yakovlev, Y. R. Padooru, G. W. Hanson, A. Mafi, and S. Karbasi, IEEE Trans. Microwave Theory Tech. **59**, 527 (2011).

[42] M. G. Silveirinha, C. A. Fernandes, and J. R. Costa, IEEE Trans. Antennas Propagat. **56**, 405 (2008).

[43] S. I. Maslovski, S. A. Tretyakov, and P. A. Belov, Microw. Opt. Technol. Lett. **35**, 47 (2002).

[44] M. G. Silveirinha and C. A. Fernandes, IEEE Trans. Microwave Theory Tech. **53**, 1418 (2005).

[45] M. G. Silveirinha, Phys. Rev. E **73**, 046612 (2006).

[46] P. Burghignoli, G. Lovat, F. Capolino, D. R. Jackson, and D. R. Wilton, IEEE Trans. Microwave Theory Tech. **56**, 1112 (2008).

[47] P. Burghignoli, G. Lovat, F. Capolino, D. R. Jackson, and D. R. Wilton, IEEE Trans. Antennas Propagat. **56**, 1329 (2008).

[48] S. I. Maslovski and M. G. Silveirinha, Phys. Rev. B **80**, 245101 (2009).

[49] M. G. Silveirinha and S. I. Maslovski, Phys. Rev. B **85**, 155125 (2012).

[50] G. W. Hanson, E. Forati, and M. G. Silveirinha, IEEE Trans. Antennas Propagat. **60**, 4219 (2012).

[51] E. Forati and G. W. Hanson, IEEE Trans. Antennas Propagat. **61**, 3564 (2013).

[52] E. Forati and G. W. Hanson, Phys. Rev. B **88**, 125125 (2013).

[53] G. W. Hanson, M. G. Silveirinha, P. Burghignoli, and A. B. Yakovlev, New J. Phys. **15**, 083018 (2013).

[54] C. R. Simovski, J. Opt. **13**, 013001 (2011).

[55] Y. Luo, A. I. Fernandez-Dominguez, A. Wiener, S. A. Maier, and J. B. Pendry, Phys. Rev. Lett. **111**, 093901 (2013).

[56] CST Microwave Studio 2009, CST GmbH, http://www.cst.com.

[57] *Spatial Dispersion in Solids and Plasmas*, edited by P. Halevi (North-Holland, Amsterdam, 1992).

[58] F. Forstmann and R. R. Gerhardts, *Metal Optics Near the Plasma Frequency* (Springer, Berlin, 1982).

[59] D. E. Fernandes, S. I. Maslovski, and M. G. Silveirinha, IEEE Trans. Microwave Theory and Tech. **62**, 8 (2014).

[60] O. Luukkonen, C. Simovski, G. Granet, G. Goussetis, D. Lioubtchenko, A. V. Risnen, and S. A. Tretyakov, IEEE Trans. Antennas Propagat. **56**, 1624 (2008).

[61] G. W. Hanson, J. Appl. Phys. **103**, 064302 (2008).